Vortex model for the nonlinear evolution of the multimode Richtmyer-Meshkov instability at low Atwood numbers

A. Rikanati
Department of Physics, Nuclear Research Center, Negev 84190, Israel
and Department of Physics, Ben Gurion University, Beer-Sheva 84015, Israel

U. Alon
Department of Physics, Nuclear Research Center, Negev 84190, Israel
and Department of Molecular Biology and Physics, Princeton University, Princeton, New Jersey 08540

D. Shvarts
Department of Physics, Nuclear Research Center, Negev 84190, Israel
(Received 10 March 1998; revised manuscript received 19 August 1998)

The nonlinear growth of the multimode Richtmyer-Meshkov instability in the limit of two fluids of similar densities (Atwood number $A \rightarrow 0$) is treated by the motion of point potential vortices. The dynamics of a periodic bubble array and the competition between bubbles of different sizes is analyzed. A statistical mechanics model for the multimode front mixing evolution, similar to the single-bubble growth and two-bubble interaction based model used by Alon *et al.* [Phys. Rev. Lett. **72**, 2867 (1994)] for $A=1$, is presented. Using the statistical bubble merger model, a power law of $t^{0.4}$ for the mixing zone growth is obtained, similar to that of the bubble front growth for the $A=1$ case and in good agreement with experiments and full numerical simulations. [S1063-651X(98)13312-3]

PACS number(s): 47.20.−k, 47.32.Cc, 02.60.Cb

I. INTRODUCTION

Hydrodynamic instabilities, such as the Rayleigh-Taylor (RT) instability [1] and the Richtmyer-Meshkov (RM) instability [2], are of crucial importance in fields like inertial confinement fusion (ICF) [3,4] and astrophysics [5]. The Rayleigh-Taylor instability occurs when a light fluid accelerates a heavier fluid while the Richtmyer-Meshkov instability occurs when a shock wave passes through an interface between the fluids. Under these instabilities, small perturbations on the initial interface develop to an array of bubbles and spikes. Recently, much progress has been made in understanding the mixing process of the RM and RT instabilities in terms of basic flow structures and their interactions [6–11]. The bubble front was found to be dominated by bubbles rising and competing; large bubbles rise faster and overtake their smaller neighboring bubbles. As a result the surviving bubbles at the front continually grow. This picture was pioneered for the RT instability by Sharp and Wheeler [6]; it was later extended by Glimm and Sharp [7]. The model of Sharp and Glimm was solved numerically by Zhang to give the correct power law for the RT bubble front in [8]. Recently such a statistical mechanics model was adopted by Alon and his coauthors [9–11] to study the late time scaling of the RM and RT instabilities in the limit of infinite density ratio (Atwood number of $A=1$). The model is based on modeling the front by an array of two-dimensional (2D) bubbles, each rising with its single-mode asymptotic velocity obtained from a Layzer-type potential flow model [12,13]. Bubbles overtake smaller neighboring bubbles to form larger bubbles (''bubble merger'') at a rate which is calculated using an extension of Layzer's potential flow model to describe two-bubble competition [10,13]. The model predicts that the bubble size spectrum, normalized to the average bubble size, reaches an asymptotically fixed distribution. Hence, at late time, the bubble-front evolution is dominated by a self-similar growth.

For $A=1$, in the case of the RT instability, the model shows that the asymptotic tip velocity of a periodic array of identical bubbles is $V=\sqrt{(1/6\pi)g\lambda}$ where λ is the bubble wavelength and g is the driving acceleration [12,13]. Furthermore, the multimode bubble front was found to grow asymptotically as $h=\alpha g t^2$ with $\alpha \cong 0.05$ in accordance with many known experimental and numerical results [14–17]. In the case of the RM instability, where the driving acceleration is impulsive in nature, the single-bubble asymptotic velocity was found to be $V=(1/3\pi)\lambda/t$ and the bubble front was found to grow according to the power law $h_b=a_0 t^{\theta_b}$ with $\theta_b \cong 0.4$, where a_0 depends on the initial perturbation mean wavelength and velocity [10,11].

At Atwood numbers smaller than one, numerical simulations and physical arguments [11] have shown that, for the RM instability, the single-mode bubble velocity maintains the form $V=C\lambda/t$ but with C having a weak dependence on A, varying from about 0.11 for $A=1$ to about 0.16 as $A \rightarrow 0$, and that the multimode bubble front still obeys the power law of $t^{0.4}$ for all Atwood numbers. These results were confirmed by full 2D numerical simulations [10,11]. Recent shock-tube experiments by Sadot *et al.* [18], have verified the single-mode bubble and spike evolution and demonstrated the bubble-competition process under shock wave acceleration for relatively high Atwood number ($A=0.7$). New, yet unpublished, results by Sadot [19] confirm the expected low Atwood number behavior by performing a similar shock-tube experiment at $A=0.2$. Impulsive acceleration

experiments were conducted by Jacobs and Sheeley [20] for a single-mode initial perturbation at $A=0.14$, verifying the low-A single-mode nonlinear evolution that is predicted by the $A=0$ vortex model, presented in that paper. Dimonte and Schnider [14] have performed impulsive acceleration experiments with random initial perturbation resulting in a $t^{0.4}$ power law for $A=0.22$.

At low Atwood numbers, when the fluids have similar densities, the mixing flow pattern is more complex than at $A=1$. Stratification and breakup of fluid drops replace the distinct bubbles and spikes of the $A=1$ case. Potential flow models, which were used to study the $A=1$ limit [9–13], do not apply in the low-A regime and an alternative approach should be used. In the present work we study the low Atwood number limit of the RM mixing zone evolution using a new vortex model, rather than the potential flow model which is used for the $A=1$ limit. The model is based on the model suggested by Jacobs and Sheeley [20] and later by Zabusky, Ray, and Samtaney [21].

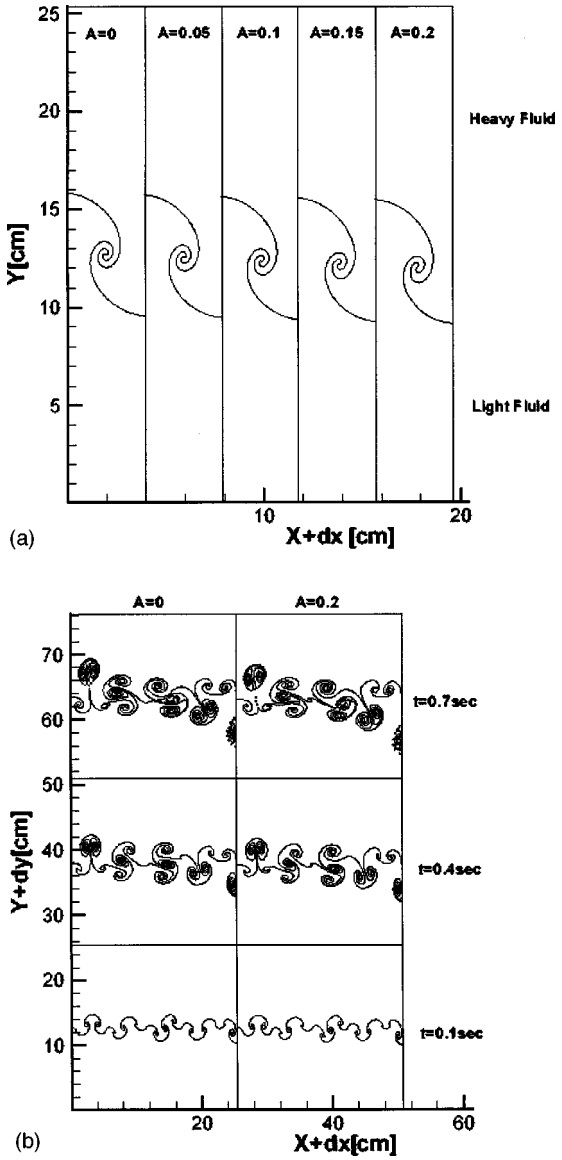

FIG. 1. Numerical comparison of the RM instability for low Atwood numbers. (a) Numerical simulations of a single-mode RM instability with $\lambda=7.7$ cm at $A=0,0.05,0.1,0.15,0.2$ and $t=0.7$ sec. For all A an identical initial velocity perturbation with an amplitude of 1 cm/sec have been imposed on the interface. The results of $A=0,0.05,0.1,0.15,0.2$ are shifted by $dx=0,\lambda/2,\lambda,3\lambda/2,2\lambda$, respectively. (b) Numerical simulations of a multimode RM instability for $A=0,0.2$. Identical initial velocity perturbation composed of a sum of 20 modes ($l=5-25$) with an average amplitude of 0.5 cm/sec is implemented for both Atwood numbers. The domain is a 26 cm×26 cm box with 200 by 200 computational cells. The results of $A=0,0.2$ are shifted by $dx=0,26$ cm and for $t=0.1$, 0.4, and 0.7 sec by $dy=0$, 26, and 52 cm, respectively.

Studying the low Atwood number limit of the RM instability, is of significance in many applications. In astrophysical systems [5], shocks are often progressing in a slowly varying density profile, and the Boussinesq low-A approximation [22] is used to describe the mixing zone evolution. In ICF, the fuel-ablator interface is usually classically unstable due to the density jump between the ablator (plastic, foam, or berilium) and the solid deuterium-tritium (DT) fuel layer [3,4,23]. The typical Atwood number at this interface is of order 0.2–0.4. In addition, calibration of effective mix models, such as the two-phase flow model [15,16,24], needs to have the right Atwood dependence in order to be applied for a general acceleration history and density profile. Having analytical limits, as well as experiments and numerical simulation results, at both high and low Atwood numbers does add to the solidity of such calibration.

Our present study is limited to the low-Mach number low-compressibility case. In such a case, the initial velocity, imprinted on the interface between the two fluids by the shock wave, is much smaller than the shock velocity. Therefore the shock wave influence on the perturbation evolution is negligible at late time [11,25,26] and the effect of the shock can be represented by an equivalent initial velocity perturbation localized around the interface. Assuming a cosine (sine) initial perturbation on the interface, the amplitude of the imprinted initial velocity perturbation is given by Richtmyer's linear theory: $U^0_{\mathrm{RM}}=kAa\Delta U$, where k is the initial perturbation wave number, A is the Atwood number, a is the initial perturbation amplitude, and ΔU is the velocity jump imprinted on the interface by the shock wave.

According to Richtmyer's theory, when A goes to zero the amplitude of the imprinted initial velocity perturbation will also go to zero. Therefore there will be no real classical RM instability at $A=0$ [27]. Yet when the interface between two fluids of equal densities ($A=0$) is subjected to a given velocity perturbation, it is still an unstable state and therefore the imposed initial perturbation will grow into a formation of a turbulent mixing zone between the two fluids, regardless of the source of the perturbation. In the present work we study the evolution of an initial velocity perturbation in the limit of $A\rightarrow 0$, aiming to represent a low-Atwood low-Mach shock wave generated instability case. In order to confirm this assumption, numerical simulations were conducted for Atwood numbers ranging from $A=0$ to $A=0.2$, both of a single-mode initial perturbation and of a multimode random initial perturbation. In the simulations an identical initial velocity perturbation was imposed on the two-fluid interface at all cases and the evolution in time of the interface was tested. The results from the simulations are shown in Fig. 1. From the simulations it is evident that both for the single-mode

case and for the multimode case, the differences between the $A=0$ results and cases of A close to zero are very small. These numerical results as well as the success of the $A=0$ vortex model in predicting the low-A experiments [19,20] strengthen our assumption that the $A=0$ case with an imposed initial velocity perturbation can serve to study the low-A low-Mach limit of the RM instability.

In the present study a vortex model for the single-bubble evolution and two-bubble interaction is constructed. The vortex model is based on extending the single-mode vortex models of Jacobs and Sheeley [20] and Zabusky, Ray, and Samtaney [21]. The model results for the single-mode and two-bubble interaction then serve in a statistical mechanics merger model to yield scaling laws for the multimode mixing zone evolution. Good agreements to the above experimental results are achieved.

II. THE VORTEX MODEL

A. Rotational flow

The RM instability is initiated by a velocity perturbation on an interface between two fluids. The initial perturbation generates an initial vorticity field. From theory [21], experiments [20], and numerical simulation of the RM instability at low Atwood numbers, one can clearly see the early formation of vortices in the flow patterns, formed by the strong attractive effective potential between vorticity points in the vorticity field. This observation implies that the flow rapidly becomes rotational rather than potential, which is the case for Atwood number $A=1$.

In fields of rotational flow the vorticity is defined as $\vec{\omega}=\vec{\nabla}\times\vec{V}$, and a vortex strength is calculated by

$$\gamma=\int_{\text{surface}}\vec{\omega}\cdot ds=\oint_{\text{contour}}\vec{V}\cdot dl, \tag{1}$$

where the surface integral is taken over the area containing the vorticity from which the vortex is generated, and the contour integral is taken over a contour limiting this area. From Kelvin's theorem of circulation the vortex strength is constant in time (viscous loss of turbulent energy is negligible under present conditions), and therefore it can be calculated from the initial velocity field.

As discussed below, in our problem we are dealing with arrays of identical bubbles, each consisting of two vortices in opposite directions. We model such an array of bubbles by a set of infinite vortex lines, as will be shown in the next section. A vortex line is described in Fig. 2.

The complex potential induced by a single vortex is [28]

$$w(z)=\left(i\,\frac{\Gamma}{2\pi}\right)\ln(z-z_0), \tag{2}$$

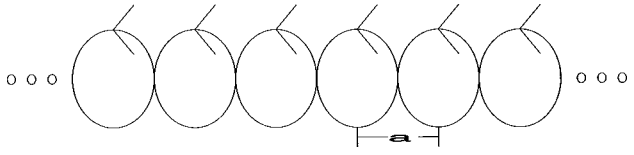

FIG. 2. A schematic drawing of an infinite vortex line where a is the distance between two neighboring vortices.

where Γ is the vortex strength, z is the complex coordinate, and z_0 is the location of the vortex in the complex field. The complex potential of a vortex line will then be [28]

$$w(z)=\sum_{n=-\infty}^{\infty}\left(i\,\frac{\Gamma}{2\pi}\right)\ln(z-na)=\frac{i\Gamma}{2\pi}\ln\sin(\pi z/a), \tag{3}$$

where a is the distance between neighboring vortices along the line and z is the complex location coordinate, $z=x+iy$. In a rotational flow field the velocity is given by $u-iv=d[w(z)]/dz$ and therefore the velocity field induced by a vortex line is

$$\begin{aligned} u(z)&=\frac{i\Gamma}{2a}\,\mathrm{Re}[\cot(\pi z/a)],\\ u(z)&=-\frac{i\Gamma}{2a}\,\mathrm{Im}[\cot(\pi z/a)]. \end{aligned} \tag{4}$$

The velocity field of a given set of vortex lines is the sum over the velocity fields induced by every line in the set.

B. Single-mode perturbation

We chose sine and cosine-type initial perturbations, which in the case of a single-mode initial perturbation is of the form

$$\begin{aligned} v(x,y)&=v_0\cos(kx)e^{-|ky|},\\ u(x,y)&=v_0\sin(kx)e^{-|ky|}. \end{aligned} \tag{5}$$

In the case of $A=0$, such an initial perturbation transforms, early in time, as seen in the simulation in Fig. 3, into a localized vortex array. This enables one to model the evolution of the single-mode initial perturbation, as described in Fig. 4, as an infinite vortex line with alternating directions, as was first suggested by Jacobs and Sheeley [20].

This line is a sum of two periodic vortex lines, described in the preceding section, and the complex potential of the line is the sum of the complex potentials of the two periodic vortex lines. The strength of the vortices forming the lines is calculated using Eq. (1), $\Gamma=4\int_0^\infty v(0,y)dy=4v_0/k$, where v_0 and k are the initial perturbation amplitude and wave number. In the case of a single-bubble array there is a full symmetry between the vortices and therefore the velocities of their centers are zero, with the result that the complex potential in the domain is a motion constant. This allows one to solve the equations for the bubble tip analytically [20]:

$$h(t)=(1/k)\sin h^{-1}(\Gamma k^2/2\pi t), \tag{6}$$

where $h(t)$ is the height of the bubble tip above the original interface. The asymptotic velocity of Eq. (6) is

$$V_{\text{asy}}=\frac{1}{2\pi}\,\frac{\lambda}{t}, \tag{7}$$

where $\lambda=2\pi/k$. The asymptotic velocity of Eq. (7) should be compared to the result at $A=1$, where $V_{\text{asy}}=(1/3\pi)(\lambda/t)$, which was derived from a potential flow

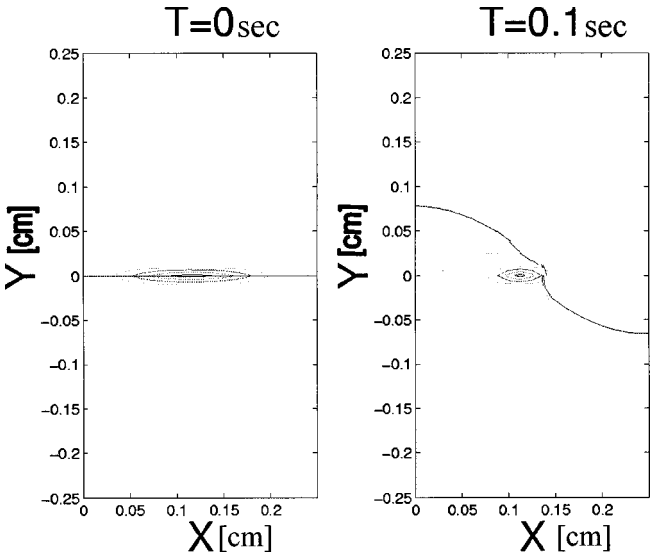

FIG. 3. Vortex formation. Vorticity contours near the bubble's interface at $t=0$ and after a short time (when the bubble's amplitude is still on the order of 0.1 of the wavelength). One can see the fast concentration of the vorticity forming a vortex. The initial perturbation is a sine with a maximum velocity of 1 cm/sec. The simulation was done with the LEEOR-2D code, a compressible ALE interface tracking code. A reflecting boundary condition was applied for the left and right sides, thus a periodic array of bubbles was simulated and the incompressible limit (high sound velocity) was used.

model by Hecht, Alon, and Shvarts [13]. The difference in the coefficient is attributed to the added mass in the $A=0$ case [29].

We compared our predictions to full scale numerical simulations, using LEEOR-2D, a compressible ALE code with interface tracking [11,16,18]. The fluid equation of state was such that the simulations were in the incompressible limit (sound velocity much greater at all times than the fluid velocities) and the density changes during the whole simulation were less than 1%.

The asymptotic velocity of Eq. (7) is compared, in Fig. 5, with a full 2D numerical simulation of a single-mode cosine perturbation with $\lambda=1$ cm and an initial bubble tip velocity of 1 cm/sec; the resolution used in the simulation was of

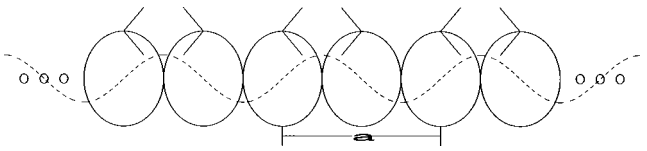

FIG. 4. Schematic drawing of two vortex lines, with a distance a between the vortices in each line and with a vortex strength $\pm\Gamma$, representing a single-bubble array perturbation. The interface perturbation is represented by a dashed line.

squared cells with 40 cells per half wavelength. The agreement between the model and the simulation is very good. As noted before, these results are also in good agreement with previous numerical simulations [11] and recent experimental results for low Atwood numbers [20,19].

Since the complex potential describes the flow in the entire domain, one can derive from Eq. (4) the velocities and the evolution in time of any point in the flow pattern. This enables one to numerically find the evolution of the whole interface by describing it as a finite set of points which can be followed numerically, by directly integrating the motion equations. The agreements between the model and the full numerical 2D simulation are very good, as can be seen in Fig. 6, for both the bubble height and the interface roll-ups inside the bubbles.

C. Two-bubble interaction

In order to model the random perturbation case with a statistical mechanics bubble-merger model we constructed a model for the interaction between two neighboring bubbles. The initial perturbation of the two bubbles is a sum of two cosines and sines of the form

$$u(x,y)=v_L\cos(k_1x)e^{-|k_1y|}+v_s\cos(k_2x)e^{-|k_2y|},$$
$$v(x,y)=v_L\sin(k_1x)e^{-|k_1y|}+v_s\sin(k_2x)e^{-|k_2y|}, \tag{8}$$

where v_L and v_S are the two bubbles' initial velocities, and k_1 and k_2 are the wave numbers from which the initial perturbation is formed. This initial perturbation describes a periodic array of bubbles of two sizes. In order to model the two-bubble interaction, the single-bubble model was ex-

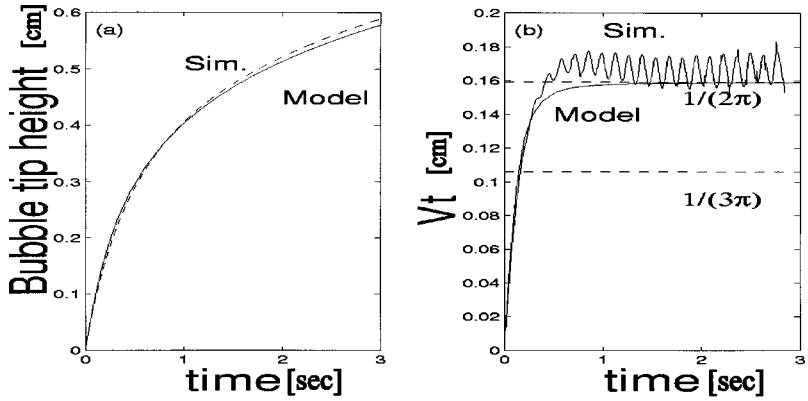

FIG. 5. Single-mode bubble height and velocity. Comparison between the model and a full 2D simulation for the case of $\lambda=1$ cm and an initial tip velocity of 1 cm/sec. (a) Bubble tip height, (b) bubble tip velocity multiplied by the time. Marked in the figure are $1/(3\pi)$ and $1/(2\pi)$, the asymptotic behavior for $A=1$ and 0, respectively. (The ripple in the simulation asymptotic velocity is due to the existence of weak sound waves that exist since the simulation fluids are not totally incompressible.) The simulation data are described in Fig. 2.

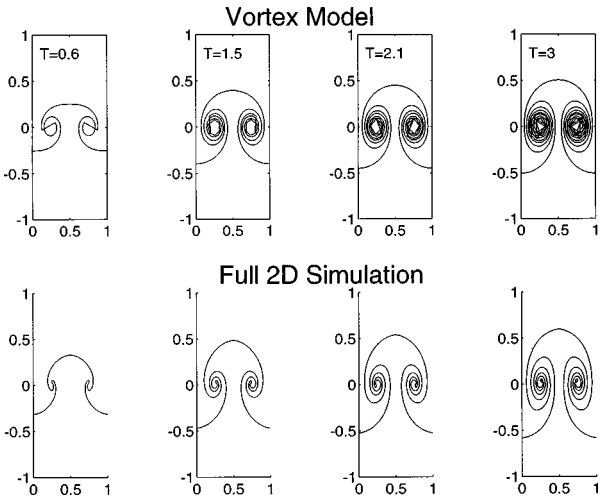

FIG. 6. Single-mode bubble interface evolution, comparison between the model and a full 2D simulation described in Fig. 2. The model results are of an ODE23 numerical calculation of 300 points from the interface. The domain is a 1 cm×1 cm box. The time is in seconds. The X and Y axes are the special X and Y coordinates and are given in cm.

tended to the case of two bubbles by setting an array of four periodic infinite vortex lines, creating an array of alternating large and small bubbles, as described in Fig. 7.

In this case the symmetry of the problem prevents relative

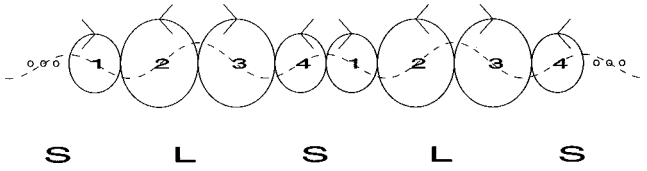

FIG. 7. Schematic drawing of four vortex lines representing a two-bubble perturbation. The perturbation is represented by the dashed line which is a sum of two cosines, L stands for a large bubble, S for a small one, and the four vortex lines are numbered 1–4. Notice that lines 1 and 3 represent vortices with a clockwise direction where line 1 is of small vortices of strength Γ_2 and line 3 is of large vortices with strengths Γ_1. Lines 2 and 4 are directed counterclockwise of strength Γ_1 and Γ_2, respectively.

motion between the vortices of a given line, but enables relative motion between the lines themselves. Thus we followed the line motion in time, where each line moves in the velocity field induced by the complex potential of the other three. In this case there are two different vortex strengths (each appearing twice, $\pm\Gamma_1$ and $\pm\Gamma_2$), as can be seen in Fig. 7. Using Eq. (1), the vortex strengths are calculated:

$$\Gamma_1 = 2\left(\frac{v_L[1+\cosh(k_1 x_m)]}{k_1} + \frac{v_s[1+\cos(k_2 x_m)]}{k_2}\right),$$
$$\Gamma_2 = 2\left(\frac{v_L[1+\cos(k_1 x_m)]}{k_1} + \frac{v_s[-1+\cos(k_2 x_m)]}{k_2}\right), \tag{9}$$

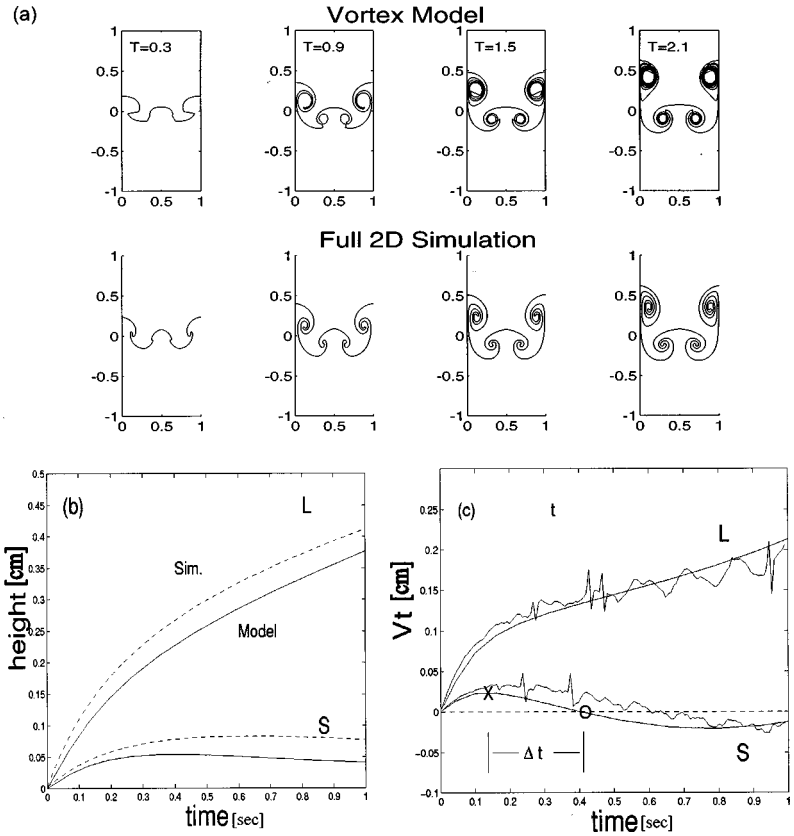

FIG. 8. Two-bubble competition. Comparison between the model and a full 2D simulation, using an ALE code with interface tracking [11], for $v_L = 1$ cm/sec and $v_S = 0.5$ cm/sec: (a) bubble interface (reflecting boundaries were used in order to simulate an array of bubbles). The time is in seconds and the X and Y axes are the special X and Y coordinates and are given in cm. (b) Bubble tip heights (dashed line—simulation, full line—vortex model). (c) Bubble tip velocity multiplied by time (smooth line—vortex model, wavy line—simulation). × indicates the beginning of the merger process, ○ the end of the merger process, and Δt is the merger time.

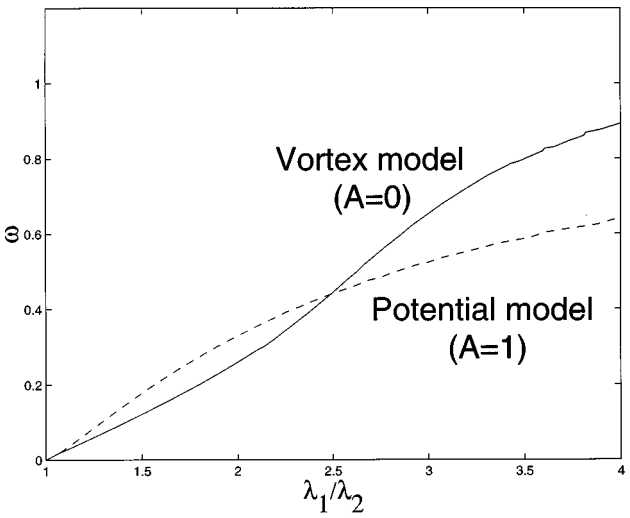

FIG. 9. Calculated dimensionless merger rate ω as a function of the wavelength ratio, for $A=0$ (full line) compared to the $A=1$ case (dashed line) [10]. The dimensionless merger rate is calculated by multiplying the merger rate by the time of the beginning of the merger.

where x_m is a reference point between the two bubbles (the point where the initial flow velocity is zero).

From the complex potential induced by the vortex lines, two equations, for the location $x_1(t),y_1(t)$ of one of the lines of the large vortices and two equations for the location $x_2(t),y_2(t)$ of the lines of the small vortices are obtained, where the locations of the other two are mirror images of the previous ones reflected on a line perpendicular to the interface, intersecting it at the tip of one of the bubbles. After numerically solving the equations one gets the motion of the vortex lines, from which the time dependent complex potential is derived in the whole domain. Using Eq. (4), the velocity history of any point can be obtained, especially that of the interface. The comparison of the model to full 2D simulations gives good results, as can be seen in Fig. 8 for $k_1=2\pi\ \mathrm{cm}^{-1}$, $k_2=4\pi\ \mathrm{cm}^{-1}$, $v_l=1$ cm/sec, and $v_s=0.5$ cm/sec.

From the model we can define the merger rate ω to be

$$\omega(\lambda_1,\lambda_2)=\frac{1}{\Delta t_{\mathrm{merger}}}, \tag{10}$$

where λ_1 and λ_2 are the wavelengths of the interacting bubbles at the beginning of the merger process and $\Delta t_{\mathrm{merger}}$ is the merger time. The merger time is the interval between the time at which the small bubble's velocity multiplied by time starts to decrease [point X in Fig. 8(c), marking the coexistence stage] and the time at which the small bubble reaches negative velocity [point O in Fig. 8(c), marking the end of the merger stage]. It was found that the merger rate depends only on the wavelength ratio $q=\lambda_1/\lambda_2$. The merger rate $\omega(q)$ is plotted in Fig. 9 and compared to the merger rate obtained by Alon *et al.* [11] for $A=1$, using the potential flow model. It can be seen that for $\lambda_1/\lambda_2<2.5$ the merger rate ω is similar for both high and low Atwood numbers while for a bubble wavelength ratio larger than 2.5 the difference is larger.

III. THE MULTIMODE BUBBLE-FRONT EVOLUTION

As mentioned in the Introduction, the RM bubble front is dominated by bubbles rising and competing. Recently, Alon and co-workers [9,10] have developed a statistical model for the RM instability in the case of $A=1$, showing that an asymptotic self-similar bubble spectrum is reached, after a few merger generations, with a power law of t^{θ} for the bubble front, where $\theta=0.4$, and in growth with a constant velocity for the spike front. In the model the bubbles are arranged along a line, and are characterized by their height h_i and their wavelength λ_i. Each bubble rises with its single-bubble velocity $V(\lambda_i,t)$ and merges with its neighboring bubbles at a merger rate $\omega(\lambda_i,\lambda_{i+1})$. The single-bubble velocity and the two-bubble merger rate were calculated using a potential flow model. The scale invariant bubble spectrum $f(\lambda/\langle\lambda\rangle)$ was introduced. The bubble front was assumed to grow with the velocity of the bubbles averaged over the scale invariant distribution:

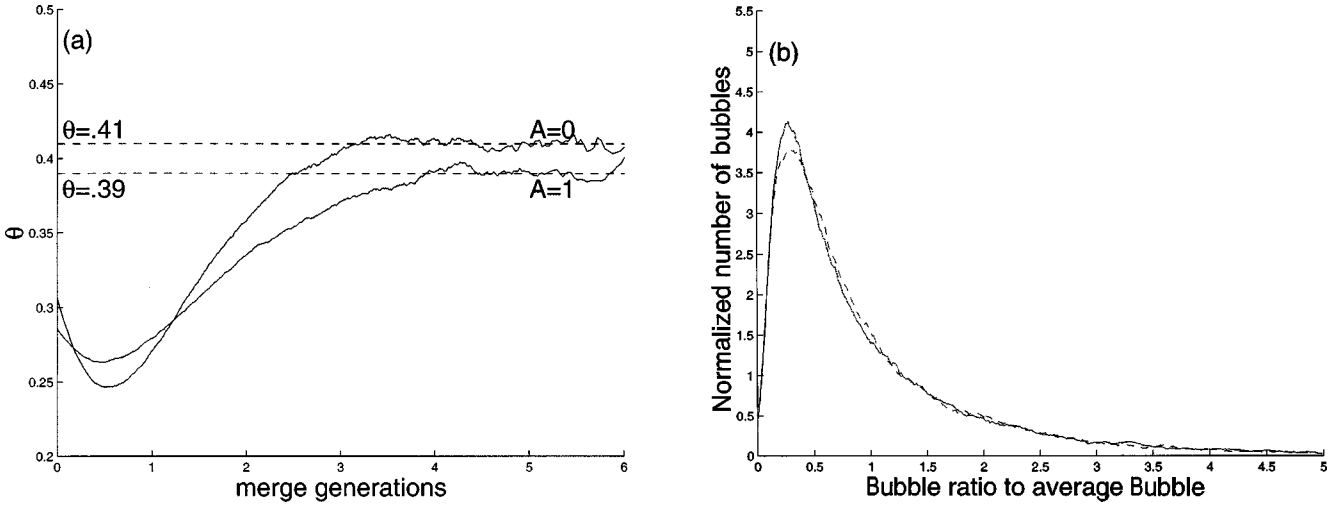

FIG. 10. Statistical merger model results, using merger rates and bubble velocities for $A=1$ and 0. (a) Turbulent mixing zone (TMZ) power-law exponent θ for $A=0$ and 1 as a function of the number of merger generations. (b) The asymptotic bubble spectrum for $A=0$ (full line) and 1 (dashed line); notice the similarity between the two.

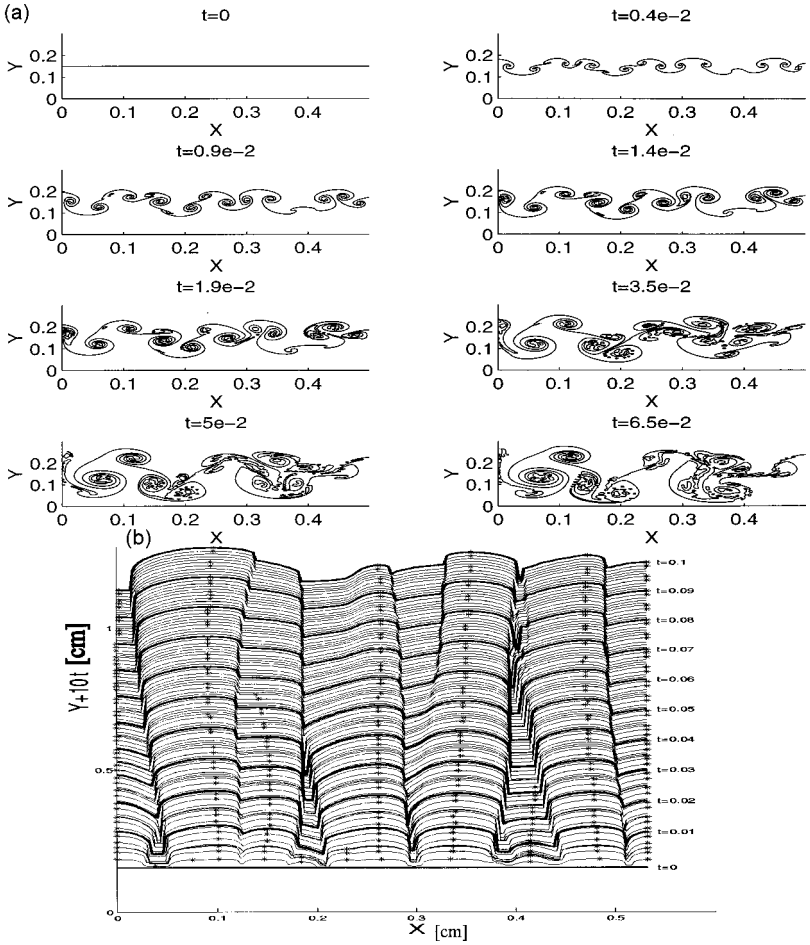

FIG. 11. Comparison between the model and a full 2D simulation for $A=0$. (a) A full 2D simulation of a 0.6 cm×0.3 cm box with 200×200 cells. Time is in seconds and x and y are in cm. (b) Simulation bubble-front top view envelope, with a time dependent Y axis displacement. The * indicates a rising bubble. One can see the bubble competition where small bubbles begin to drop and larger ones take over the space of the smaller ones.

$$d\langle h\rangle_f/dt=\langle V_1(\lambda,t)\rangle_f, \tag{11}$$

with $\langle h\rangle_f=\int h(\lambda,t)f(\lambda)d\lambda$ and $\langle V_1(\lambda,t)\rangle_f=\int V(\lambda,t)f(\lambda)d\lambda$.

Applying the results from the vortex model for the single-bubble velocity of Eq. (7), Eq. (11) becomes $d\langle h\rangle/dt=\langle\lambda\rangle_f/(2\pi t)$. The average wavelength increases as $\langle\lambda\rangle_f=L/N(t)$, where L is the total length of the domain and N is the number of rising bubbles. From the average merger rate the time dependence of the number of bubbles is derived:

$$dN(t)/dt=\langle\omega\rangle N(t). \tag{12}$$

Integrating Eq. (11) with Eq. (12) the bubble-front height $h_b(t)$ is derived:

$$h_b(t)=a_0t^\theta, \tag{13}$$

with $\theta=\langle\omega\rangle_f$ and $a_0=c\overline{\lambda_0}^{1-\theta}\overline{v_0}^\theta$, where c is a dimensionless constant, $\overline{\lambda_0}$ is the mean wavelength of the initial bubble ensemble, and $\overline{v_0}$ is the mean velocity of the bubble ensemble [11]; the form of a_0 can be derived from simple dimensional considerations. Therefore the Richtmyer-Meshkov instability power-law exponent is $\theta=\langle\omega\rangle_f$ where the average is taken over the bubble spectrum f, $\theta=\int\omega(x,y)f(x)f(y)dxdy$.

In order to study the RM $A\to0$ limit, we used the statistical model, based on the results of the vortex model for the single-bubble velocity and for the two-bubble merger rate. The statistical model was applied numerically for an initial ensemble of 100 000 bubbles distributed with $f(\lambda)=$const for $\lambda\in[0.5\text{ cm},1.5\text{ cm}]$ and zero otherwise. The bubbles were set along a line with each pair of neighboring bubbles having a probability of merger proportional to $\omega(q)$ of Eq. (10). After three to four merger generations (i.e., each surviving bubble has merged three to four times), an asymptotic self-similar bubble distribution was achieved. From the bubble spectrum and $\omega(q)$ the average merger rate is calculated and the power of the bubble-front height growth rate is derived using Eq. (13). In Fig. 10 one can see the results of the statistical model. It is seen that asymptotically, after about three to four merger generations when a self-similar regime is reached, θ approaches the value $\theta_{\text{asy}}=0.41$ for $A=0$ as compared to $\theta_{\text{asy}}=0.39$ for $A=1$. The results for $A=1$ are calculated using $V_{\text{asy}}=(1/3\pi)\lambda/t$ and $\omega(q)$ as was derived by Alon *et al.* [10] using the potential flow model.

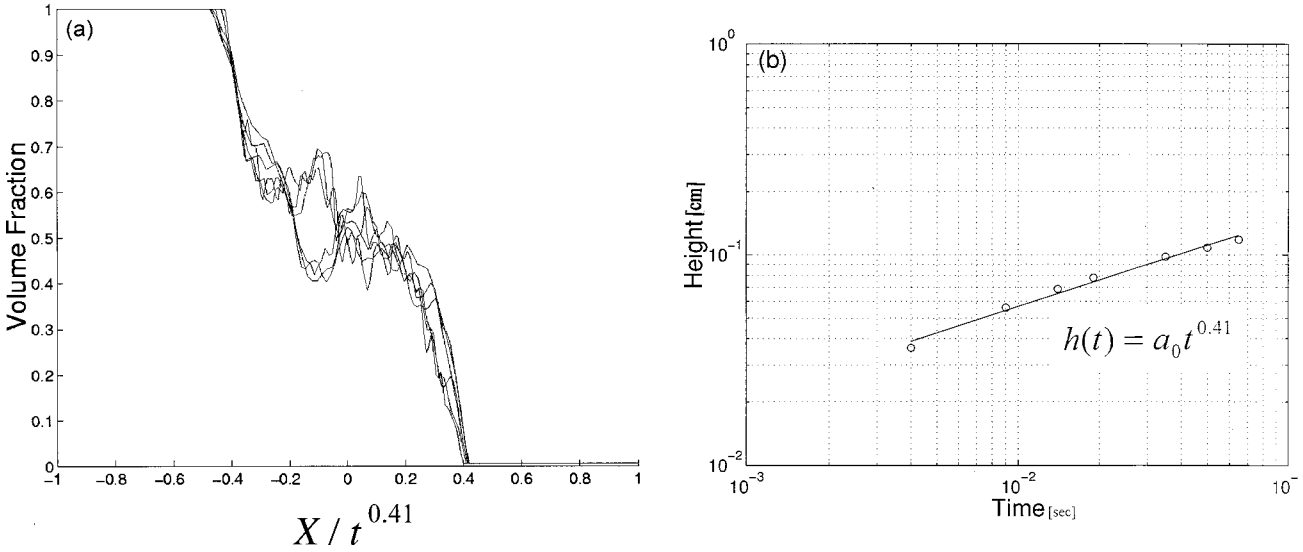

FIG. 12. Comparison between the model and a full 2D simulation for $A=0$. (a) TMZ volume fraction at several times, where the X axis is $X/t^{0.4}$. One can see the self-similar behavior of the TMZ. (b) Bubble-front height calculated at 10% mass fraction.

It is found that the bubble-front growth rate exponent is similar for both $A=1$ and 0. The reason for this is that θ is determined by the merger rate $\omega(q)$, which, as can be seen in Fig. 9, is similar in both cases for the main region of the self-similar bubble spectrum, $\lambda_1/\lambda_2<2.5$. In the RM case the growth rate is similar for all A because while in the RT case the buoyancy force term, which depends linearly on A, leads to a linear dependence of the bubble-front height coefficient on $A(\alpha_{\text{bubble}}=0.05A)$, in the RM case, where only the weakly A dependent drag force is controlling the late time evolution [11], the growth rate exponent should be similar for all A. Note that even though the bubble front does grow similarly in the $A=0$ and 1 cases, there is a large difference in the evolution of the whole mixing zone region between these two cases due to the large differences in the spike front scaling: at $A=0$, bubbles and spikes are symmetrical and go as $t^{0.4}$, while at $A=1$, spikes are growing linearly in time. In general at $0<A<1$, $\theta_{\text{spike}}>\theta_{\text{bubble}}$. For more detail see [11].

The result for the evolution of a random initial perturbation at $A=0$ was compared to a full 2D simulation. The simulations have been conducted with the ALE code LEEOR-2D with a 200×100 cell mesh covering a $0.5\ \text{cm}\times0.25\ \text{cm}$ domain. The initial condition was a velocity perturbation on the interface which is the sum of 20 modes with random amplitudes:

$$v(x,y)=\sum_{n=1}^{20} v_n\cos(k_n x)e^{-|k_n y|}u(x,y)$$

$$=\sum_{n=1}^{20} v_n\sin(k_n x)e^{-|k_n y|}, \tag{14}$$

where v_n are random numbers, $0<v_n<1$.

The occurrence of bubble competition is clearly seen in Fig. 11. The $t^{0.4}$ self-similarity of the horizontally averaged volume fraction from the simulation is seen in Fig. 12(a) and the 10% averaged volume fraction location in time, seen in Fig. 12(b), does obey the $t^{0.4}$ power law, in very good agreement with the model predictions. Recently this result was confirmed experimentally for low Atwood numbers in [14].

IV. CONCLUSION

Using a vortex model for the Richtmyer-Meshkov instability for Atwood number $A=0$, we model the single-bubble velocity to get the asymptotic value $v_{\text{asy}}=1/2\pi\lambda/t$ and the complex interaction between two neighboring bubbles. Using a statistical model we describe the development of random perturbations based on the mechanism of bubble merger. This leads to the power law of $t^{0.4}$, as in the previously studied $A=1$ case [10], supporting the conclusion that the power-law exponent for the RM instability bubble front is independent of the Atwood number. Note that for the spike front, an Atwood number dependent power law was found [10]. At $A\to0$ bubbles and spikes become symmetric and the entire mixing zone grows as $t^{0.4}$.

It is remarkable that similar large-structure physics appear to determine the mixing zone evolution at both density ratio extremes. In both extremes simplifying conditions allowed us to derive the large-structure behavior (potential flow model at $A=1$ and vortex model at $A=0$). This method, describing a complex flow by quantifying its simple fluid structures and their pair interactions, might offer a powerful tool for the study of other mixing processes.

The result for the power-law exponent of the evolution of the RM instability is an important result and is related to many fields of turbulence, such as the Kelvin-Helmholtz instability, turbulent decay [30], etc. The power-law exponent for the RM instability, $\theta\cong0.4$, was recently used, together with the RT instability constant of $\alpha_b\cong0.05$ [11], to construct an effective mix model for predicting the growth rates of hydrodynamic instabilities [24].

[1] Lord Rayleigh, Proc. London Math. Soc. **14**, 170 (1883); reprinted in *Scientific Papers of Lord Rayleigh* (Cambridge University Press, Cambridge, England, 1900), Vol. II, p. 200.
[2] R. D. Richtmyer, Commun. Pure Appl. Math. **13**, 297 (1960); E. E. Meshkov, Fluid Dyn. (USSR) **4**, 101 (1969).
[3] S. W. Haan, S. M. Pollaine, J. D. Lindl, L. J. Suter, R. L. Berger, L. V. Powers, W. E. Alley, P. A. Amendt, J. A. Futterman, W. K. Levedahl, M. D. Rosen, D. P. Rowley, R. A. Sacks, A. I. Shestakov, G. L. Strobel, M. Tabak, S. V. Weber, G. B. Zimmerman, W. J. Krauser, D. C. Wilson, S. V. Coggeshall, D. B. Harris, N. M. Hoffman, and B. H. Wilde, Phys. Plasmas **2**, 2480 (1995).
[4] J. D. Lindl, Phys. Plasmas **2**, 3933 (1995).
[5] T. Ebisuzki, T. Shigeyama, and K. Nomoto, Astron. J. **344**, L65 (1989); I. Hachisu, T. Matsuda, K. Nomoto, and T. Shigeyama, Astrophys. J. Lett. **368**, L27 (1991); L. Smarr, J. R. Wilson, R. T. Barton, and R. L. Bowers, *ibid.* **246**, 515 (1981); J. Arons and S. M. Lea, *ibid.* **207**, 914 (1976); F. Catteneo and S. M. Hughes, J. Fluid Mech. **196**, 323 (1988); E. A. Frieman, Astrophys. J. **120**, 18 (1954); S. V. Sazanov, Planet. Space Sci. **39**, 1667 (1991); W. S. D. Wilcock and J. A. Whitehead, J. Geophys. Res. **96**, 12 193 (1991).
[6] D. H. Sharp, Physica D **12**, 3 (1984).
[7] J. Glimm and D. H. Sharp, Phys. Rev. Lett. **64**, 2137 (1990).
[8] Q. Zhang, Phys. Lett. A **151**, 18 (1990).
[9] U. Alon, D. Shvarts, and D. Mukamel, Phys. Rev. E **48**, 1008 (1993).
[10] U. Alon, J. Hecht, D. Mukamel, and D. Shvarts, Phys. Rev. Lett. **72**, 2867 (1994).
[11] U. Alon, J. Hecht, D. Ofer, and D. Shvarts, Phys. Rev. Lett. **74**, 534 (1995).
[12] D. Layzer, Astrophys. J. **122**, 1 (1955).
[13] J. Hecht, U. Alon, and D. Shvarts, Phys. Fluids **6**, 4019 (1994).
[14] G. Dimonte and M. Schneider, Phys. Rev. E **54**, 3740 (1996).
[15] D. L. Youngs, Physica D **12**, 32 (1984); **37**, 270 (1989).
[16] N. Freed, D. Ofer, D. Shvarts, and S. A. Orszag, Phys. Fluids A **3**, 912 (1991).
[17] K. I. Read, Physica D **12**, 45 (1984).
[18] O. Sadot, L. Erez, U. Alon, D. Oron, L. A. Levin, G. Erez, G. Ben-Dor, and D. Shvarts, Phys. Rev. Lett. **80**, 1654 (1998).
[19] O. Sadot, Ph.D. thesis, Ben-Gurion University, 1998.
[20] J. W. Jacobs and J. M. Sheeley, Phys. Fluids **8**, 405 (1996).
[21] N. Zabusky, J. Ray, and R. S. Samtaney, in *Proceedings of the 5th International Workshop on Compressible Turbulent Mixing*, edited by R. Young, J. Glimm, and B. Boyton (World Scientific, Singapore, 1995).
[22] S. Chandrasekhar, *Hydrodynamic and Hydromagnetic Stability* (Oxford University Press, New York, 1968), Chap. II.
[23] S. E. Bodner, D. G. Colombant, J. H. Gardner, R. H. Lehmberg, S. P. Obenschain, L. Phillips, A. J. Schmitt, J. D. Sethian, R. L. McCrory, W. Seaka, C. P. Verdon, J. P. Knauer, B. B. Afeyan, and H. T. Powel, Phys. Plasmas **5**, 1901 (1998).
[24] U. Alon and D. Shvarts, in *Proceedings of the 5th International Workshop on Compressible Turbulent Mixing*, edited by R. Young, J. Glimm, and B. Boyton (World Scientific, Singapore, 1995).
[25] Y. Yang, Q. Zhang, and D. Sharp, Phys. Fluids **6**, 1856 (1994).
[26] Q. Zhang and S. I. Sohn, Phys. Lett. A **212**, 149 (1996); Phys. Fluids **9**, 1106 (1997).
[27] The statement is correct in the incompressible limit, yet in the compressible regime in cases where the hydrodynamic impedance of the two fluids is different (for example, two ideal gases with different adiabatic indices) a shock wave will generate a velocity perturbation on the interface leading to RM instability growth.
[28] A. R. Paterson, *A First Course in Fluid Dynamics* (Cambridge University Press, Cambridge, England, 1983).
[29] L. Arazi (private communication).
[30] U. Alon, S. A. Orszag, and D. Shvarts had suggested that from a power law of $t^{0.4}$ one can derive the empirical turbulence decay power law of $t^{-1.2}$ (unpublished).